Q. J. R. Meteorol. Soc. (1994), **120**, pp. 453–482 551.510.413.2:551.513.1

A three-dimensional model study of nitrogen oxides in the stratosphere

By D. J. LARY, J. A. PYLE* and G. CARVER
University of Cambridge, UK

(Received 25 November 1992; revised 29 July 1993)

SUMMARY

A new three-dimensional model for stratospheric chemistry studies is described. The model, a spectral general circulation model, is developed from the model used at the European Centre for Medium-range Weather Forecasts. Schemes to describe atmospheric chemistry and photochemistry as well as advection of trace gases have been implemented. In this study a perturbed period in January 1987 is studied. The model performs well. An interesting feature, similar to the Noxon cliff, is reproduced in which the NO_2 column is reduced significantly in high latitudes. In this calculation the cliff is produced by gas phase conversion of NO_2 to N_2O_5.

1. INTRODUCTION

It was first suggested in the early 1970s that stratospheric ozone could be depleted by a variety of man-made compounds (Johnston 1971; Crutzen 1971; Molina and Rowland 1974). Projections of the likely ozone loss were based first on one-dimensional photochemical models, which consider only the variation in species concentration with altitude (see the references above), and subsequently on two-dimensional (2-D) models (e.g. Pyle 1980). The latter models include transport by the mean meridional circulation, but eddy transport, associated with large-scale atmospheric waves, must be parametrized. Some 2-D models have included the feedback between ozone amount, radiative heating and the meridional circulation (e.g. Harwood and Pyle 1975), but many have not. In either case there is a fundamental limitation in describing a three-dimensional (3-D) system with only two spatial variables (see, for example, Murgatroyd (1982) for a detailed discussion).

The years since ozone loss was first hypothesized have seen the atmospheric chemistry community become more aware of the importance of an adequate description of 3-D atmospheric transport. With increases in computing power a number of atmospheric chemistry studies that use 3-D models have been performed. Early studies included Mahlman and Moxim (1978) who introduced a very simple 'ozone-like' tracer into their general circulation model (GCM). Cariolle and Deque (1986) developed a highly parametrized ozone scheme for their model, which produced a very satisfactory ozone distribution. Subsequently, other stratospheric chemistry schemes of varying sophistications have been included into 3-D models (e.g. Grose *et al.* 1987; Kaye and Rood 1989; Rood *et al.* 1990; Granier and Brasseur 1991; Austin and Butchart 1992).

The steady increase in computer power has now led to a situation where integrations of stratospheric chemistry schemes in 3-D models are quite feasible for process studies. On the other hand, integrations covering many decades for assessment studies are not yet practical unless run at very low resolution, but such integrations can be expected before long, especially as the importance for climate change of ozone modification in the lower stratosphere is now recognized (see, for example, Lacis *et al.* 1990).

This paper describes the first results with a new 3-D stratospheric chemistry model, based on a GCM from the European Centre for Medium-range Weather Forecasts (ECMWF), which is being developed as a climate/atmospheric chemistry research tool

* Corresponding author: Centre for Atmospheric Science, Department of Chemistry, University of Cambridge, Lensfield Road, Cambridge CB2 1EW, UK.

by the UK Universities Global Atmospheric Modelling Programme (UGAMP). Various modifications to the model have been effected to allow the inclusion of atmospheric chemistry. These are described in section 2, where the model is discussed in more detail. Section 3 contains a description of the chemistry and photochemistry schemes included for this integration. The model described here includes detailed treatments of the chemistry that involve ozone and the nitrogen-, hydrogen- and chlorine-oxide families. A description of the overall performance of the chemical model in a two-week integration initialized dynamically in mid-January 1987 is given in section 4. Emphasis is given to an analysis of the nitrogen budget in the model. A feature resembling the Noxon cliff, in which there is a sharp decrease in the NO_2 column as the pole is approached, is found; this is dealt with in more detail and its causes discussed in section 5. Our conclusions are given in section 6.

2. The UK UGAMP general circulation model

The UK UGAMP GCM (UGCM) is a full 3-D primitive-equation model, based on the ECMWF cycle 27 GCM (Tibaldi *et al.* 1990). The model includes a detailed set of parametrizations for unresolved dynamical and physical processes. The UGCM differs from the ECMWF cycle 27 version mainly by the inclusion of a facility for tracer advection and a detailed stratospheric chemistry scheme, described below. The model was run on the Cray XMP/48 at the Atlas Computer Centre at the Rutherford Appleton Laboratory.

The primitive equations are expressed in terms of vorticity, divergence, temperature, specific humidity and log surface pressure. The spectral technique (Hoskins and Simmons 1975) is used to solve the equations in the horizontal, whilst a finite-difference scheme is used in the vertical. For this study the UGCM was run with a triangular truncation of the retained modes in wave-number space up to zonal wave number 21 (usually written as T21). This corresponds approximately to a grid of $6° \times 6°$ in latitude and longitude. Physical parametrizations are calculated in grid-point space and then transformed to spectral space. The hybrid sigma–pressure vertical coordinate of Simmonds and Burridge (1981) is used, in which the lowest model levels are sigma levels whilst the uppermost are pressure levels. The model has 19 levels in the vertical, from the surface up to 10 mb. The resolution in the stratosphere is relatively coarse, with levels at approximately 10, 30, 50, 75, 100 and 140 mb. The earth's orography is spectrally fitted and smoothed before being included as a boundary condition in the model.

The semi-implicit time integration scheme of Hoskins and Simmons (1975) with an Asselin (1982) time filter is used. At a horizontal resolution of T21 the dynamical time step would normally be 45 minutes, but stable integration of the chemical scheme (forward Euler) required a 5-minute time step. In this study, therefore, a 5-minute step was used for the integration of both chemistry and dynamics. Our more recent work has used an implicit scheme for the chemistry, allowing longer time steps. Solution of the radiative-transfer equation to compute the radiative fluxes is performed once every 3 hours on a reduced grid to save computer time. All other physics parametrizations (including radiative heating rates) are calculated at each step on the full model grid.

Horizontal diffusion is applied in spectral space to all the model's prognostic variables, using a sixth-order operator with an 8-hour e-folding time at wave number 21. Horizontal diffusion is increased for the top five model levels to provide a 'sponge-layer' with a 15-minute e-folding time at the top level for wave number 21. This is necessary to control the large wind speeds that would otherwise develop. It has the consequence of removing small-scale features, but the large-scale features are unaffected. Vertical diffusion, based on Monin–Obukhov similarity theory, is also applied in the planetary

boundary layer and in the free atmosphere dependent on the stability. The radiation parametrization includes short- and long-wave fluxes in clear and cloudy sky conditions. It allows for partial cloud cover in any model layer and includes multiple scattering (Geleyn and Hollingsworth 1979; Geleyn *et al.* 1982). A separate radiative code, described later, is used for the photolysis-rate calculations. Convection is modelled using a modified version of the Kuo (1974) scheme. Shallow convection is treated as part of the model's vertical diffusion (Tiedtke 1983).

For the UGAMP research a tracer advection facility was incorporated in the model. This allows passive or chemically active tracers to be advected in the model, using the model winds updated on each time step. This 'on-line' calculation allows, for example, the possibility of incorporating the modelled species fields into the radiation parametrization, although this was not done for this study. The tracer advection code was written so that the maximum number of tracers is limited only by the available computer memory. In practice more than 30 tracers becomes prohibitive.

The tracer advection is discretized, using the spectral method in the horizontal and the finite-difference scheme in the vertical as for the other prognostic variables. However, it is well known that the spectral method suffers deficiencies when representing fields with large horizontal gradients over a few grid points (Rood 1987). These are often highlighted by the occurrence of negative mixing-ratio values and regions of undershoot and overshoot where the minimum or maximum mixing-ratio value is exceeded, although conservation globally is ensured. There are two main causes of these problems. First, the grid associated with a spectral truncation supports more waves than is actually used by the model; thus small-scale information on the grid can be lost. Second, Gibbs phenomena can occur when discontinuities develop in the field; this has important consequences for chemical source regions. For distributions of chemical species in which sharp gradients form (such as those with a pronounced diurnal cycle) the spectral technique may not be the most appropriate, and numerical errors will arise.

The vertical advection scheme can also produce undershoot and overshoot since it is first-order accurate with the model's variable vertical spacing. The vertical advection scheme can also give rise to regions of negative mixing-ratio values.

We have taken a very crude approach in these first calculations to the problem of negatives by simply setting negative values to zero. This, of course, leads to non-conservation, which would be very serious in a long integration but is acceptable in the short run presented here. Our recent model developments have included an improved scheme for vertical advection (Thuburn 1993), which significantly reduces the problem, as well as a borrowing scheme in the chemistry that ensures conservation.

3. Stratospheric photochemical scheme

(*a*) *The chemistry scheme*

A comprehensive photochemical package containing 74 chemical and photochemical reactions is used to describe the stratospheric chemistry of O_x, NO_x, HO_x and ClO_x (Table 1). The rate constants were taken from DeMore *et al.* (1987). The rapid time-scales on which certain photochemical processes occur can impose a severe limitation on the time step that must be used in chemical models if numerical stability is to be maintained. A well proven technique, which provides a computational solution to this as well as a conceptual simplification, is the family approach, in which continuity equations are solved for a family, and not for species individually. A family is a group of constituents that are in photochemical equilibrium with each other. The interchange between family

TABLE 1. REACTIONS CONSIDERED

(1)	$O + O_2 \xrightarrow{M} O_3$	(41)	$O + HOCl \rightarrow OH + ClO$
(2)	$O + O_3 \rightarrow 2O_2$	(42)	$N + NO \rightarrow N_2 + O$
(3)	$O(^1D) + N_2 \rightarrow O(^3P) + N_2$	(43)	$N + O_2 \rightarrow NO + O$
(4)	$O(^1D) + O_2 \rightarrow O(^3P) + O_2$	(44)	$CCl_4 + O(^1D) \rightarrow 4Cl$
(5)	$O(^1D) + H_2O \rightarrow 2OH$	(45)	$CH_3CCl_3 + O(^1D) \rightarrow 3Cl$
(6)	$OH + O \rightarrow H + O_2$	(46)	$CH_3CCl_3 + OH \rightarrow 3Cl$
(7)	$O_2 + H \xrightarrow{M} HO_2$	(47)	$CH_3Cl + O(^1D) \rightarrow Cl$
(8)	$HO_2 + O \rightarrow OH + O_2$	(48)	$CH_3Cl + OH \rightarrow Cl$
(9)	$OH + O_3 \rightarrow HO_2 + O_2$	(49)	$CHF_2Cl + O(^1D) \rightarrow Cl$
(10)	$H + O_3 \rightarrow OH + O_2$	(50)	$CHF_2Cl + OH \rightarrow Cl$
(11)	$OH + HO_2 \rightarrow H_2O + O_2$	(51)	$CF_2ClCFCl_2 + O(^1D) \rightarrow 3Cl$
(12)	$OH + OH \rightarrow H_2O + O$	(52)	$NO_3 + NO_2 \xrightarrow{M} N_2O_5$
(13)	$NO_2 + O \rightarrow NO + O_2$	(53)	$N_2O_5 \xrightarrow{M} NO_3 + NO_2$
(14)	$NO + O_3 \rightarrow NO_2 + O_2$	(54)	$ClO + ClO \xrightarrow{M} Cl_2O_2$
(15)	$NO_2 + O_3 \rightarrow NO_3 + O_2$	(55)	$Cl_2O_2 \xrightarrow{M} ClO + ClO$
(16)	$HNO_3 + OH \rightarrow NO_3 + H_2O$	(56)	$O_2 + h\nu \rightarrow O + O$
(17)	$NO_2 + OH \xrightarrow{M} HNO_3$	(57)	$O_3 + h\nu \rightarrow O_2 + O(^3P)$
(18)	$N_2O + O(^1D) \rightarrow 2NO$	(58)	$O_3 + h\nu \rightarrow O_2 + O(^1D)$
(19)	$HO_2 + HO_2 \rightarrow H_2O_2 + O_2$	(59)	$NO + h\nu \rightarrow N + O$
(20)	$H_2O_2 + OH \rightarrow H_2O + HO_2$	(60)	$NO_2 + h\nu \rightarrow NO + O(^3P)$
(21)	$OH + CH_4 \rightarrow CH_3 + H_2O$	(61)	$NO_3 + h\nu \rightarrow NO + O_2$
(22)	$O(^1D) + CH_4 \rightarrow CH_3 + OH$	(62)	$NO_3 + h\nu \rightarrow NO_2 + O$
(23)	$NO + HO_2 \rightarrow NO_2 + OH$	(63)	$HNO_3 + h\nu \rightarrow NO_2 + OH$
(24)	$HO_2 + O_3 \rightarrow OH + 2O_2$	(64)	$N_2O_5 + h\nu \rightarrow NO_2 + NO_3$
(25)	$HO_2 + NO_2 \xrightarrow{M} HO_2NO_2$	(65)	$HO_2NO_2 + h\nu \rightarrow NO_2 + HO_2$
(26)	$HO_2NO_2 \xrightarrow{M} HO_2 + NO_2$	(66)	$N_2O + h\nu \rightarrow N_2 + O(^1D)$
(27)	$HO_2NO_2 + OH \rightarrow H_2O + O_2 + NO_2$	(67)	$ClONO_2 + h\nu \rightarrow Cl + NO_3$
(28)	$CFCl_3 + O(^1D) \rightarrow 3Cl$	(68)	$CCl_4 + h\nu \rightarrow 4Cl$
(29)	$CF_2Cl_2 + O(^1D) \rightarrow 2Cl$	(69)	$CFCl_3 + h\nu \rightarrow 3Cl$
(30)	$Cl + O_3 \rightarrow ClO + O_2$	(70)	$CF_2Cl_2 + h\nu \rightarrow 2Cl$
(31)	$ClO + O \rightarrow Cl + O_2$	(71)	$CHF_2Cl + h\nu \rightarrow Cl$
(32)	$ClO + NO \rightarrow Cl + NO_2$	(72)	$CF_2ClCFCl_2 + h\nu \rightarrow 3Cl$
(33)	$CH_4 + Cl \rightarrow CH_3 + HCl$	(73)	$HOCl + h\nu \rightarrow Cl + OH$
(34)	$H_2 + Cl \rightarrow H + HCl$	(74)	$Cl_2O_2 + h\nu \rightarrow ClO_2 + Cl \rightarrow 2Cl + O_2$
(35)	$HO_2 + Cl \rightarrow O_2 + HCl$		
(36)	$OH + HCl \rightarrow H_2O + Cl$		
(37)	$ClO + NO_2 \xrightarrow{M} ClONO_2$		
(38)	$ClONO_2 + O \rightarrow$ products		
(39)	$HO_2 + ClO \rightarrow HOCl + O_2$		
(40)	$OH + HOCl \rightarrow H_2O + ClO$		

members occurs in a time-scale that is much less than the net production/loss time-scale of the family as a whole. Since the photochemical lifetime of the family is greater than any of its individual members, a computational advantage results, because numerical stability can be maintained with much longer model time steps than would otherwise be possible. Furthermore, since the role of atmospheric transport is generally easier to identify in the global distribution of the family, rather than for individual family members, a conceptual simplification occurs.

A careful choice of family members is very important since, if the assumption of photochemical equilibrium is not valid over the whole model domain, quite large errors can be incurred (e.g. Douglass *et al.* 1989; Austin 1991). This problem must be avoided by a careful analysis of the lifetimes of the constituents involved. Generally, if the lifetime of a given constituent exceeds a few hours, caution should be exercised in its inclusion

in a family. For example, photolysis of N_2O_5 can be rapid at low latitudes in the stratosphere; N_2O_5 has a short lifetime and could be included in a family along with NO and NO_2. However, N_2O_5 photolysis is slow (or zero) at high latitudes during winter, the lifetime of N_2O_5 increases and so an assumption of immediate photochemical equilibrium with NO and NO_2 is no longer valid.

An additional factor in deciding the family members is the relative importance of the particular constituents. For example, in some circumstances up to 50% of the total reactive nitrogen can be in the form of N_2O_5, so that a careful treatment of N_2O_5 is essential. However, another constituent of comparable lifetime to N_2O_5 is HO_2NO_2, but HO_2NO_2 is present at much lower concentrations (typically $< 1\%$ of the nitrogen species) so that a slight departure from photochemical equilibrium for HO_2NO_2 would not have such a large potential impact.

An analysis of stratospheric lifetimes was conducted and this led to the choice of families given in Table 2. With two exceptions the families listed in Table 2 are transported by the model winds as described in the previous section. First, as in the Cambridge 2-D model, HO_x is assumed to be in photochemical equilibrium, and is not transported by the model winds. This is a good approximation, since HO_x has a very short lifetime in the troposphere and stratosphere. If this assumption is not made, then the time step that would be required for numerical stability (< 1 minute) is such that the model could not be used for integrations of much longer than one day. Second, in the short integration described here, the long-lived source gases are not transported but are simply specified.

The continuity equation is solved for each family. For example,

$$\frac{\partial[O_x]}{\partial t} = \sum_i P_i - \sum_i L_i[O_x] - \nabla(\mathbf{r}[O_x]) \tag{1}$$

where the photochemical production rate of O_x is denoted by ΣP_i, the chemical destruction rate of O_x is denoted by $\Sigma L_i\,[O_x]$, and $\mathbf{r}$ is the wind vector. Once this equation is solved for the concentration of O_x, the concentration of the family members (O_3, $O(^1D)$ and $O(^3P)$) are calculated by using the family ratios

$$\frac{[O(^1D)]}{[O_3]} = \frac{j_{58}}{k_3[N_2] + k_4[O_2]} \tag{2}$$

$$\frac{[O(^3P)]}{[O_3]} = \frac{j_{57} + j_{58}}{k_1[O_2][M]} \tag{3}$$

$$\frac{[O_3]}{[O_x]} = \frac{1}{1 + \dfrac{[O(^3P)]}{[O_3]} + \dfrac{[O(^1D)]}{[O_3]}} \tag{4}$$

where j is the photolysis rate, k the thermal reaction, M stands for any third body involved in a reaction and the square brackets denote concentrations.

A more detailed description of the model is given by Lary (1991). The kinetic data are taken from DeMore *et al.* (1990), apart from the following: the absorption cross-section for the Herzberg continuum of molecular oxygen is taken from Nicolet and Kennes (1986) and WMO (1986); the absorption cross-section for the Schumann–Runge bands of molecular oxygen are calculated using the parametrization of J. E. Frederick (1985, private communication) (see also WMO 1986); the temperature dependence of the O_3 absorption cross-section in the spectral region $264\text{ nm} < \lambda < 345\text{ nm}$ is calculated using a quadratic fit to the dataset of A. M. Bass presented by J. E. Frederick (1985, private communication) (see also WMO 1986); the absorption cross-sections of NO in

the δ(0-0) and δ(1-0) bands are calculated using the parametrization of Allen and Frederick (1982). This parametrization applies for the region above 20 km, and for solar zenith angles up to 85°. Outside this domain the parametrization does not apply, and the absorption cross-section is set to zero. The temperature-dependent absorption cross-sections of the halocarbons CH_3Cl, CCl_4, F11($CFCl_3$), F12(CF_2Cl_2), and F22(CHF_2Cl) are calculated using the parametrizations of Simon *et al.* (1988) (although the impact of this photolysis is of course negligible in the very short integration discussed below).

The stratospheric chemistry scheme is being continually developed and updated. Our most recent studies include yet more detailed chemical packages, for example the chemistry of the bromine compounds. Nevertheless, the scheme presented here is quite sufficient for the detailed study of the nitrogen oxides presented below.

(*b*) *Radiative transfer model*

The radiative transfer model used in this study to calculate atmospheric photolysis rates is a new implementation of the scheme described by Meier *et al.* (1982). It has been extended after Anderson (1983) to describe correctly the radiation field for solar zenith angles greater than 75°. The radiation into any volume element of the model atmosphere has four contributions: (A) the direct solar flux, (B) the diffuse flux incident from all directions, (C) the ground reflection of the direct solar flux, and (D) the ground reflection of the diffuse flux. This is illustrated schematically in Figure 1.

The radiation field is calculated by solving the integral equation of radiative transfer. The detailed mathematical description of the four contributions is described by Meier *et al.* (1982) and Lary (1991). The direct flux is treated by using a full spherical geometry, and the scattered flux by the plane-parallel approximation. Using the plane-parallel approximation to describe the multiple scattering, results in an underestimate of the radiation field for solar zenith angles greater than 93°. We have usually carried calculations up to 96°, with some loss of accuracy at the largest angles. The accuracy of the method has been demonstrated by Anderson (1983). Our implementation has been justified by a number of studies that compare the chemistry/radiative model with atmospheric measurements (Lary 1991; Lary *et al.* 1991; Lary and Pyle 1991a, b). The studies presented in this paper assume clear sky conditions.

Photolysis rates are calculated by making use of an enhancement factor, or normalized source function, S_λ (Meier *et al.* 1982), defined as the total number of photons,

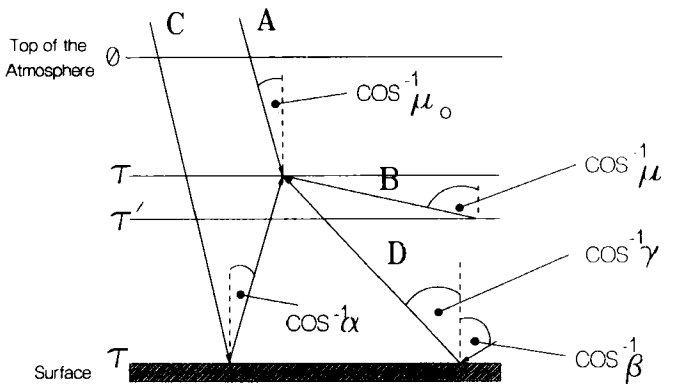

Figure 1. Schematic diagram of the radiative-transfer model used for the calculation of photolysis rates. (Adapted from Meier *et al.* (1982) and reproduced from Lary and Pyle (1991a) with the permission of the *Journal of Atmospheric Chemistry*).

F_λ, integrated over all directions, which is available for photolysis at any given point in the atmosphere, normalized by the number of photons incident at the top of the atmosphere, $F_{0\lambda}$,

$$S_\lambda = \frac{F_\lambda}{F_{0\lambda}}. \tag{5}$$

Any photolysis rate j, can readily be calculated from a knowledge of the solar flux incident at the top of the atmosphere, $F_{0\lambda}$, the absorption cross-section, σ_λ, the quantum efficiency, ϕ_λ, and the enhancement factor, S_λ, using

$$j_i(z, \chi, A_{\text{ground}}) = \int F_{0\lambda} S_\lambda(z, \chi, A_{\text{ground}})\, \phi_{\lambda_i}\, \sigma_{\lambda_i}\, \mathrm{d}\lambda. \tag{6}$$

Note that the enhancement factor S_λ is a function of wavelength λ, solar zenith angle χ, altitude z, and ground albedo A_{ground}. S_λ also depends on which ozone, temperature and aerosol profiles are used. In this study atmospheric aerosols have not been included, and a single ozone and temperature profile was used in the calculations of the photolysis rates. Studies conducted more recently have used the local profiles.

4. Results

For the initial run with the model described above we have carried out a study of the evolution of the dynamical and chemical fields in a 14-day integration during a disturbed northern hemisphere winter.

The model was initialized dynamically with the ECMWF analysis for 12 GMT 15 January 1987 and integrated for two weeks. There are no global datasets available for this period to initialize the chemistry. We have, therefore, taken the simplest possible approach. The chemical fields were initialized from the Cambridge 2-D model. Thus, initially, the chemical fields were zonally symmetric, an unrealistic condition and a point discussed further later.

(*a*) *Dynamical fields*

The stratosphere of January 1987 was perturbed by an extremely intense mid-winter warming that developed early in the month and persisted well into February. The details of the warming are described by Naujokat *et al.* (1987). During mid to late January the main features changed little: a pronounced wave-number one pattern at 10 mb, with a corresponding geopotential height minimum of about 28 km centred over northern Scandinavia and Russia, moved only very slowly to the south-west during this period. Figure 2 shows the 10 mb geopotential maps for 19, 21 and 27 January derived from Stratospheric Sounding Unit (SSU) data. Temperature fields are shown in Fig. 3. Temperatures at the pole are high in late January, as shown in the temperature map for 19 January at 10 mb (Fig. 3(b)). Notice the very strong temperature gradients with very low temperatures associated with the vortex over northern Scandinavia.

The model dynamics were initialized during the warming; we can, therefore, make no statement about the prediction of the onset of the perturbation. The model, even at the low resolution used, followed the observed features reasonably well, especially during the first week of the integration. (Similarly good agreement over about the first week of integration was found in studies of the 1991/92 winter, see Carver *et al.* (1994).) Figure 4 shows the calculated 10 mb geopotential heights for 19, 21 and 27 January. The geopotential minimum on 19 January was about 28.6 km, slightly higher than inferred

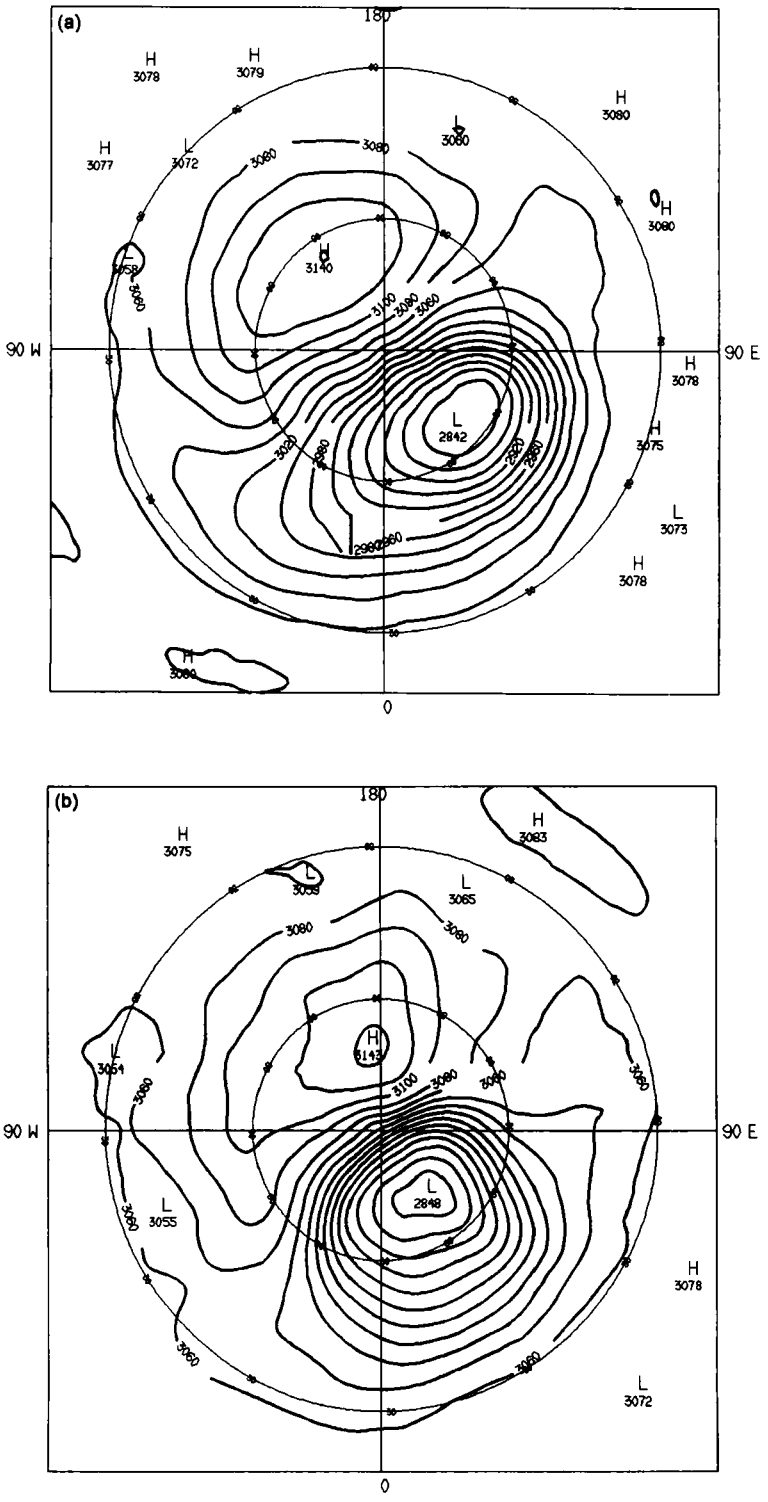

Figure 2. Geopotential heights (dagpm) for the northern hemisphere 10 mb surface from SSU data for: (a) 19 January 1987, (b) 21 January 1987, and (c) 27 January 1987. (Courtesy of Drs A. O'Neill and M. Bailey, Meteorological Office).

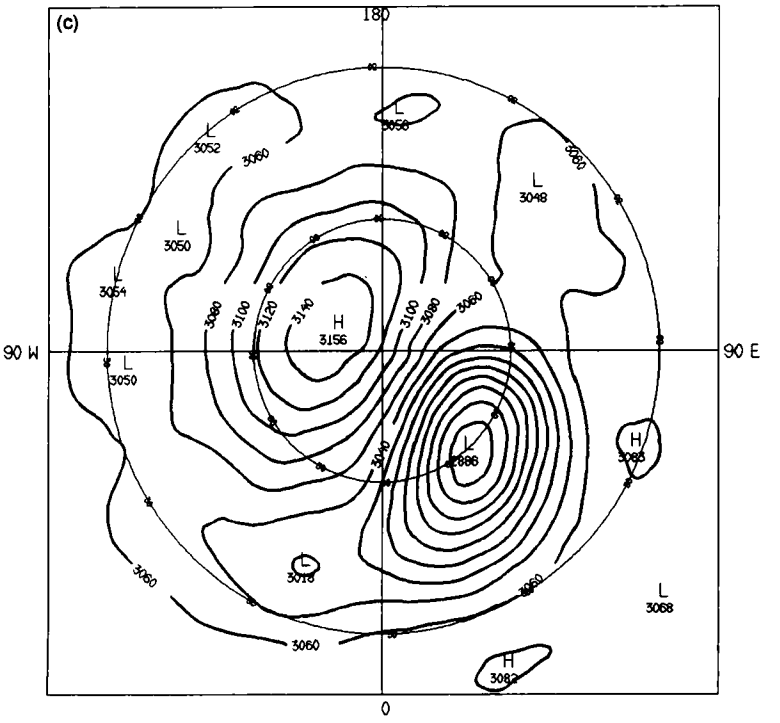

Figure 2. Continued.

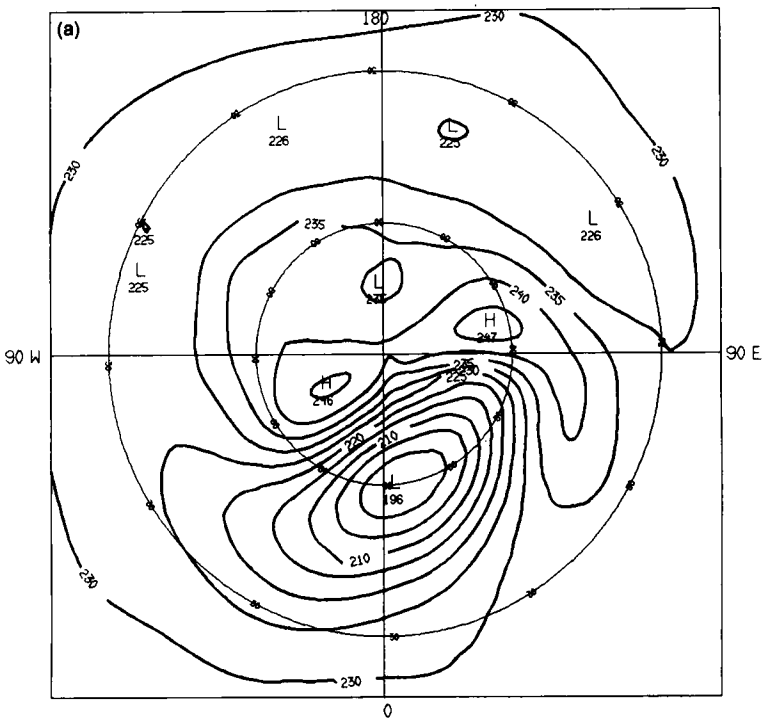

Figure 3. As Fig. 2 but for temperatures (K).

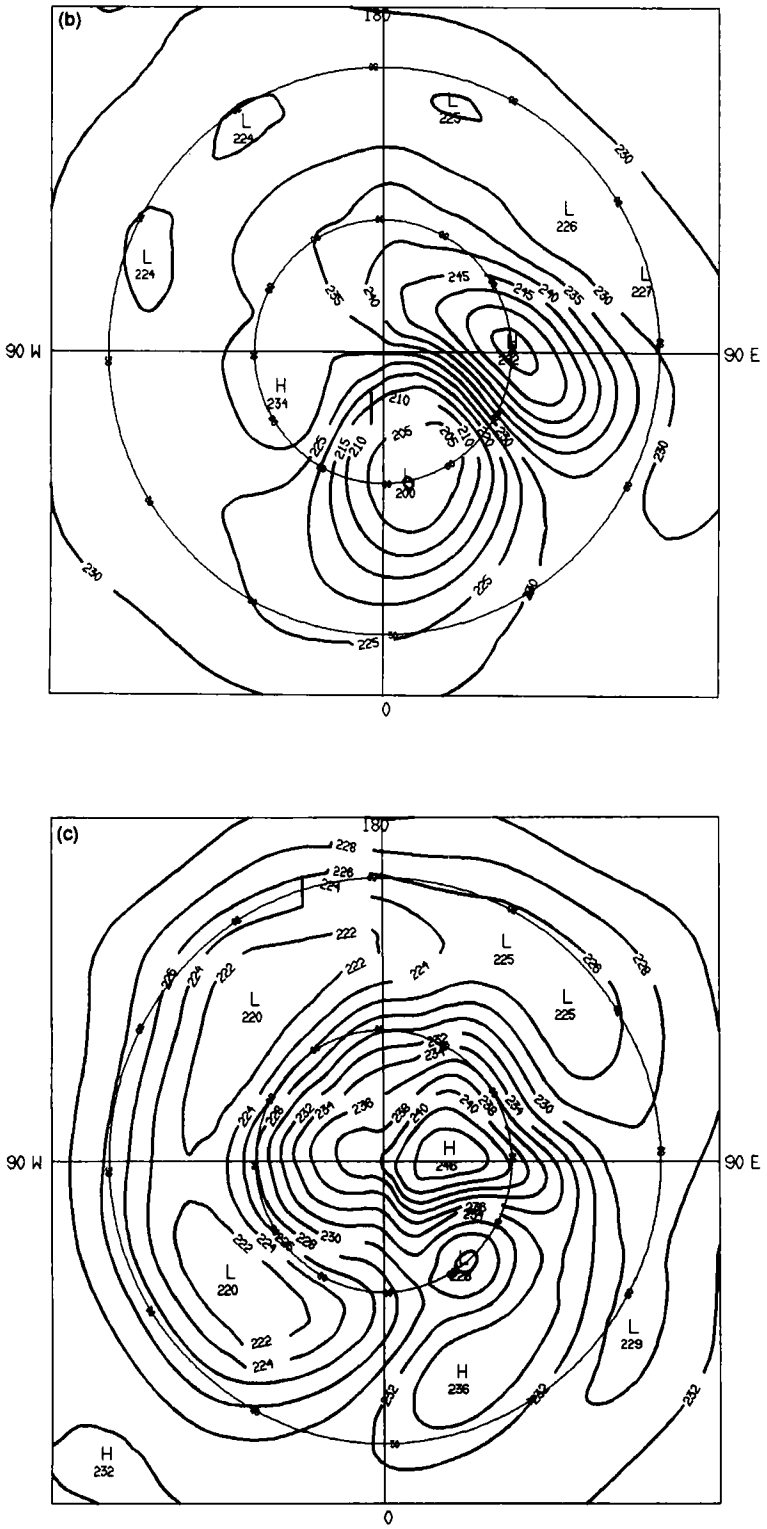

Figure 3. Continued.

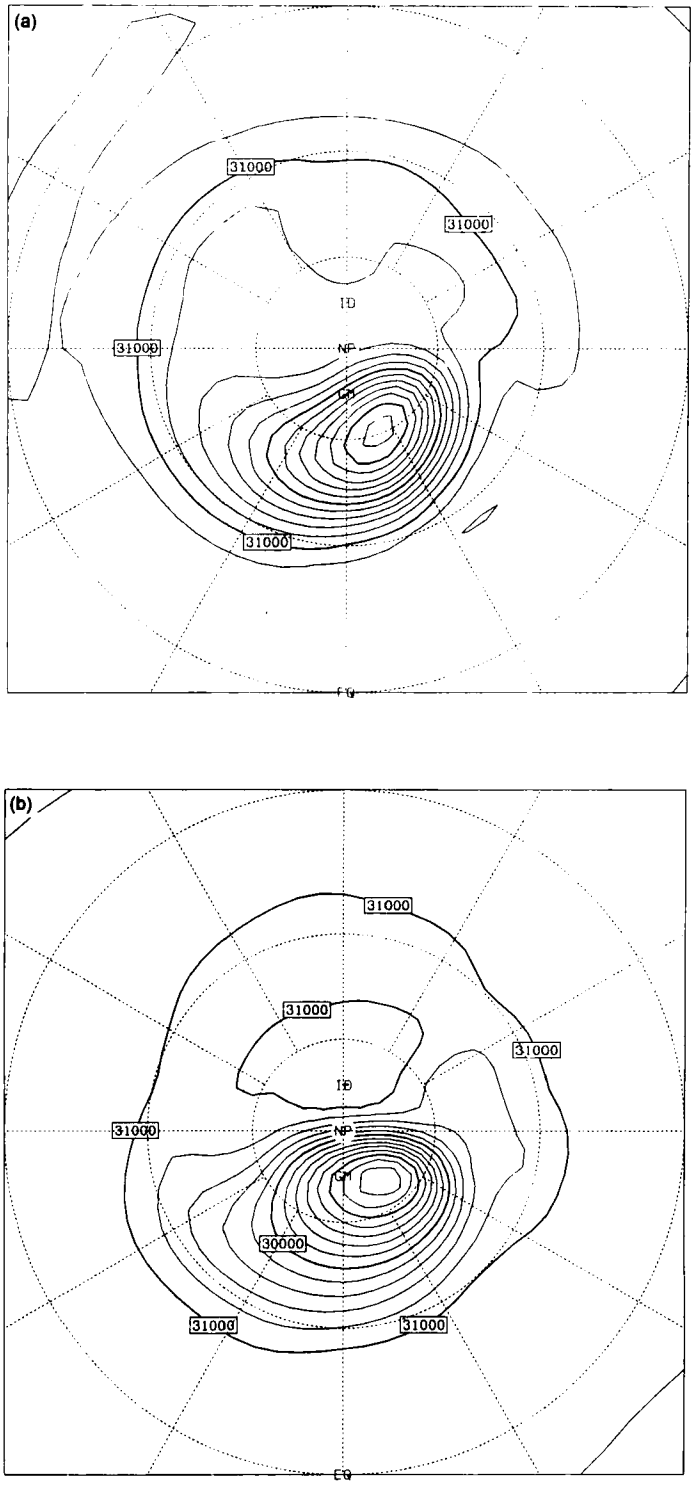

Figure 4. Calculated geopotential heights for the northern hemisphere 10 mb surface for: (a) 19 January 1987, (b) 21 January 1987 and (c) 27 January 1987. Contours every 200 kgpm.

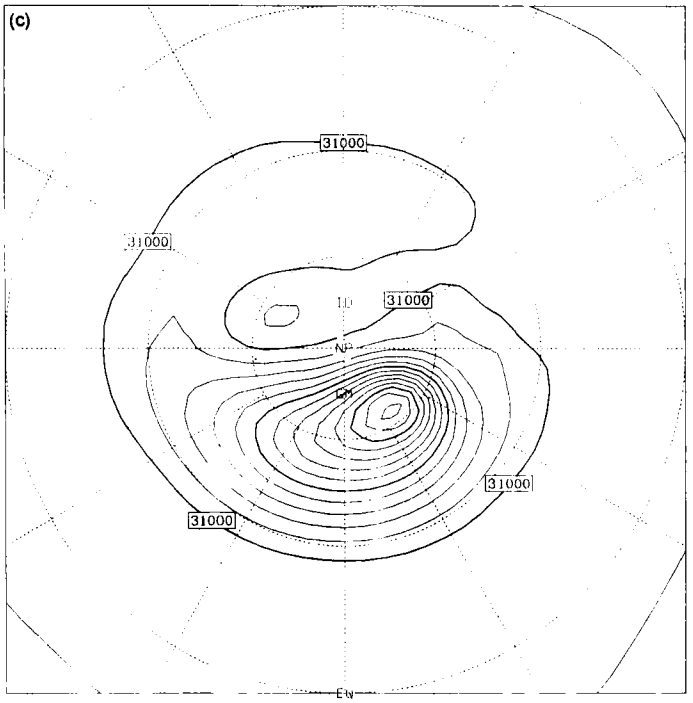

Figure 4. Continued.

from SSU data. The position and orientation of the modelled vortex agree quite well with the observations. On 21 January the agreement is even better, with the position and magnitude of the observed and modelled geopotential minimum coinciding almost exactly. By 27 January, at the centre of the vortex, the geopotential height was about 28.6 km, lower than observed. The modelled vortex extends much further across the Greenwich meridian than observed (Fig. 2(c)) and the high-pressure system is not reproduced particularly well. Nevertheless, the model retains the main feature of the observations, with a vortex centred over the European sector.

The model 10 mb temperatures on 19, 21 and 27 January are shown in Fig. 5. Notice that the lowest temperatures in the sequence are found on 19 January, being less than 200 K, and that on both 19 and 21 January high temperatures are observed over the pole. By 27 January the lowest temperature had increased to nearly 210 K, with the temperature minimum moving south and west during the integration. These features are qualitatively similar to those shown in the observed temperature field (see Fig. 3), although by 27 January the observed structure looks quantitively quite different to that observed. In particular, the high temperatures observed close to the pole are considerably underestimated in the model integration.

Our objective in this paper is not to discuss in detail the dynamical behaviour of the model during this particular period up to the end of January 1987. Instead we want to discuss some aspects of the chemical behaviour of the model during a disturbed winter period. For this purpose it is not, of course, necessary that the integration bears any resemblance to the observed circulation, particularly as there are few chemical observations against which to compare the model during this same period. Nevertheless, it is clear from the above that the dynamical model did indeed perform quite well in a predictive role during this period.

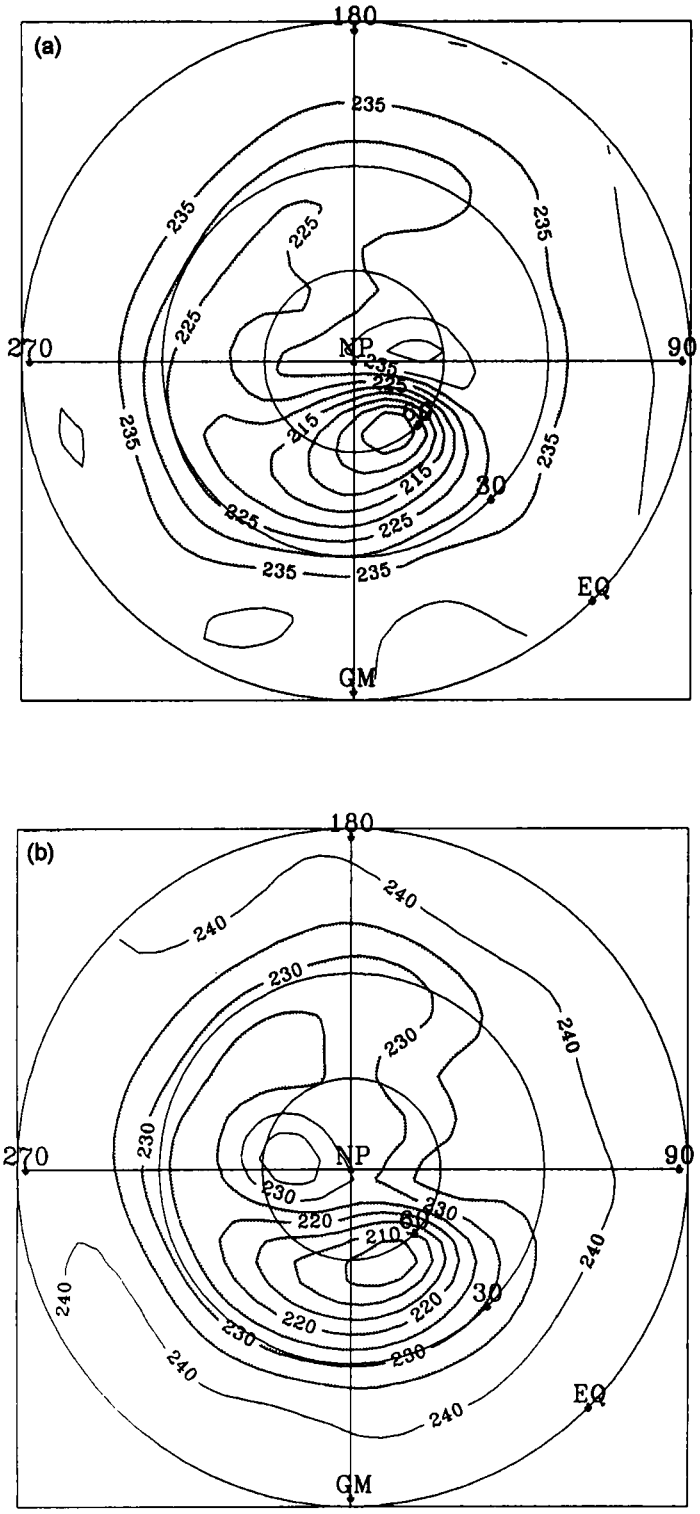

Figure 5. As Fig. 4 but for calculated temperature (K).

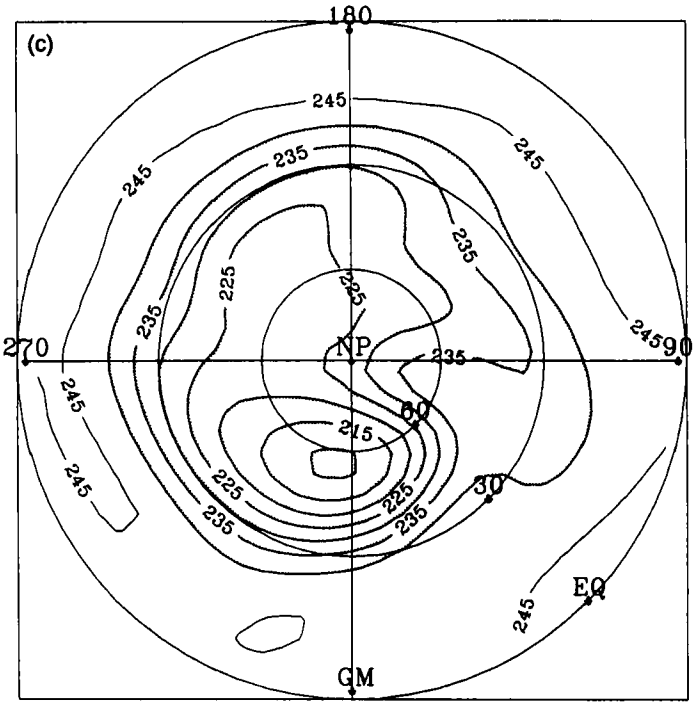

Figure 5. Continued

(*b*) *Total ozone*

Figure 6 shows the calculated vertical ozone column for 15, 17 and 19 January. Notice that the largest contribution to the ozone column comes in the lower stratosphere, where the vertical resolution of the model is relatively poor.

The model begins with a zonally symmetric ozone field, but very quickly a complicated structure is developed and by 19 January the maximum values form an H-shape stretching from the North American continent across the pole to central Russia. On this day much lower values of ozone are found over the United Kingdom and Scandinavia. Figure 7 shows a Total Ozone Measuring System (TOMS) map for 19 January 1987. There is excellent qualitative and quantitative agreement between these observations and the model results (Fig. 6(c)). For example, the model maximum of nearly 500 Dobson units (DU) at 60°N, 120°E can be compared with a TOMS maximum also of 500 DU in the same region. Such good agreement may seem surprising at first sight, since the initially zonally symmetric conditions were quite unlike the atmospheric state. However, the ozone column is determined largely by atmospheric dynamics. For example, the inverse correlation between total ozone and tropopause height has been known for many years (Dobson *et al.* 1927). (Vaughan and Price (1991) have recently pointed to an even better correlation between total ozone and the vorticity around the tropopause level.) The good comparison between model and data arises simply from a realistic dynamical representation of the lower stratosphere soon after initialization with the correct meteorological analysis. This is confirmed by Fig. 8 that shows the model 100 mb geopotential height for 19 January. Notice the extremely good correspondence between the orientation across the pole of the geopotential minimum and the ozone column (Figs.

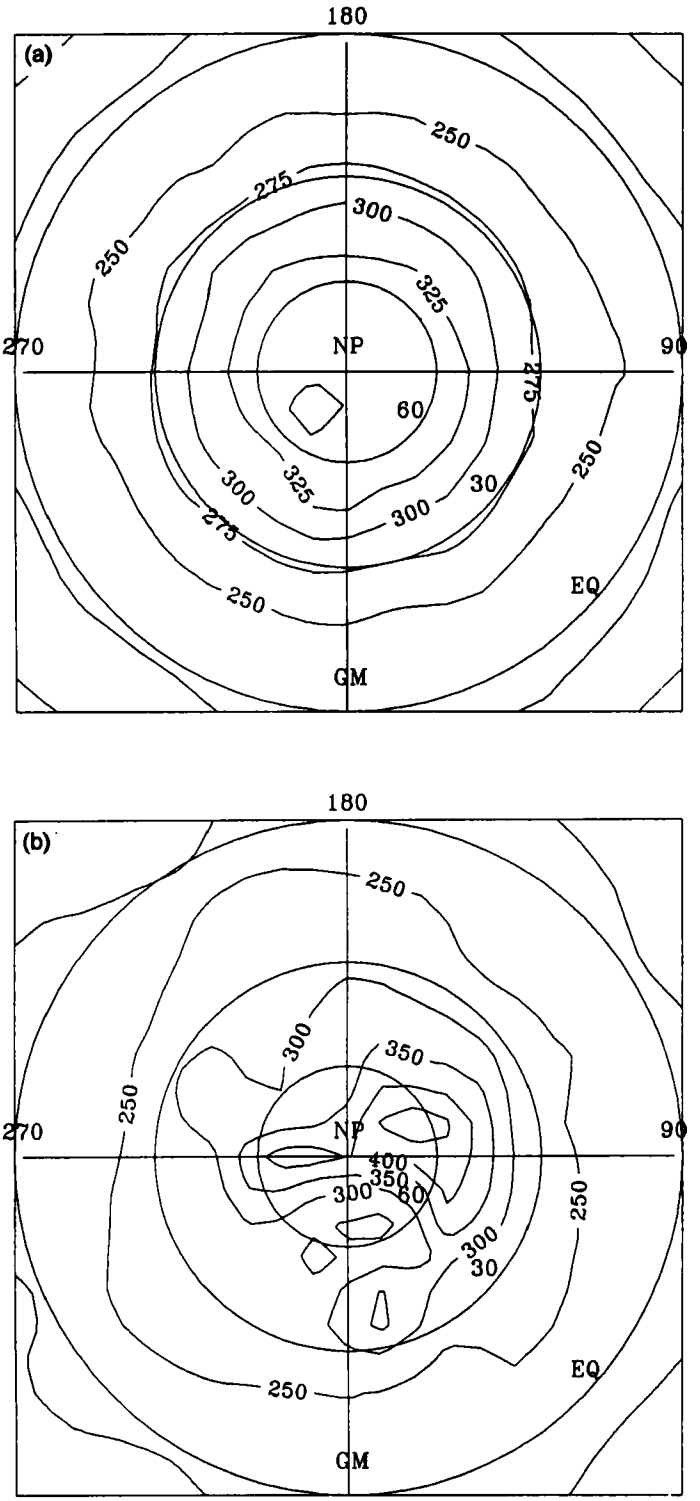

Figure 6. The northern hemisphere total ozone column (DU) for: (a) 1400 GMT 15 January 1987, (b) 1200 GMT 17 January 1987, (c) 1200 GMT 19 January 1987.

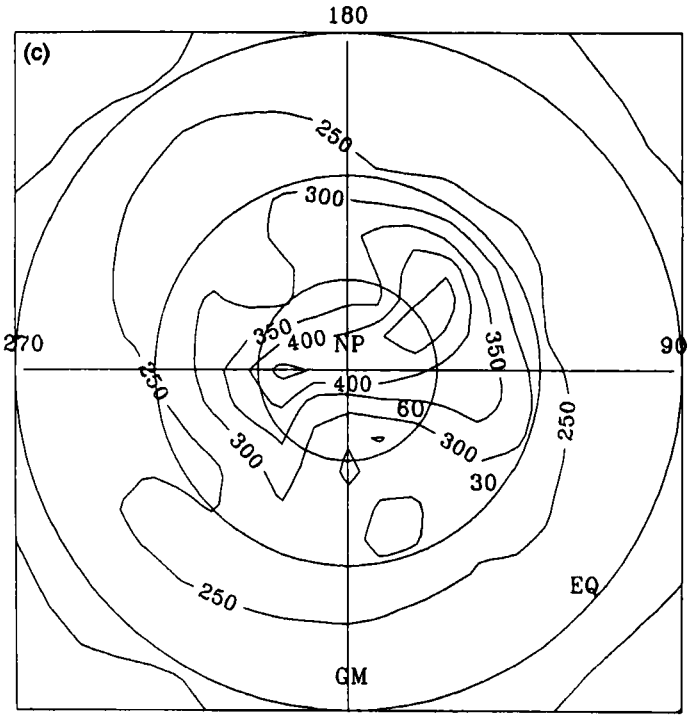

Figure 6. Continued.

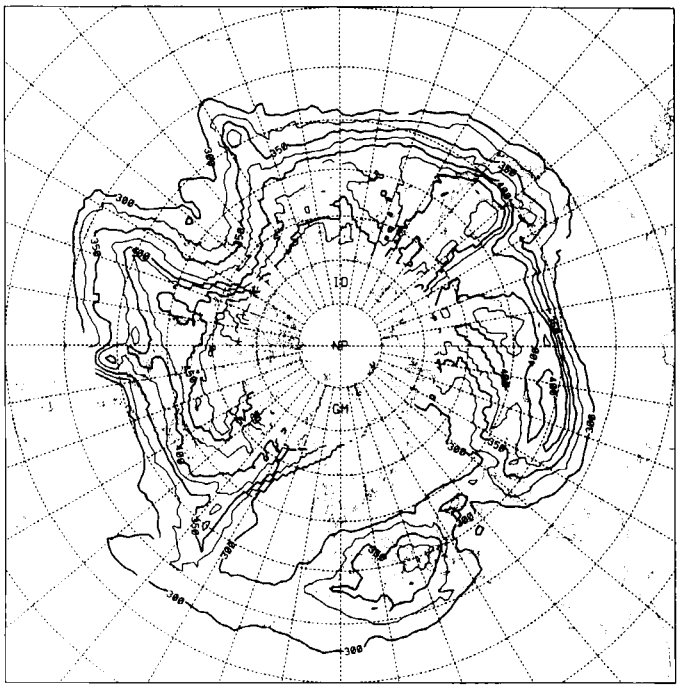

Figure 7. The northern hemisphere total ozone column as observed by the TOMS instrument on 19 January 1987.

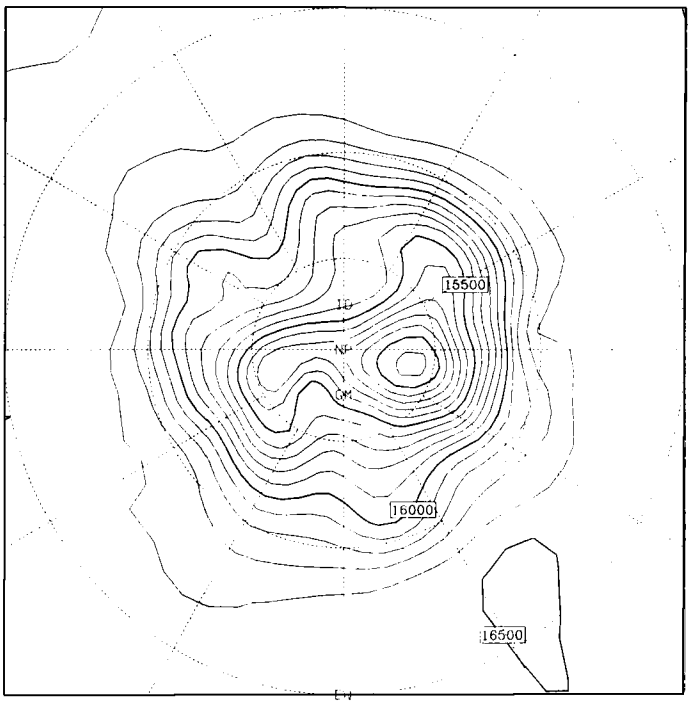

Figure 8. Modelled geopotential height for the northern hemisphere 100 mb surface on 19 January 1987. Contours every 100 kgpm.

6(c) and 7). Notice also that the arms of the H-shape in the modelled total ozone correspond to the geopotential minimum over North America and Siberia.

At later dates in the integration, detailed comparison between TOMS observations and the model become less good. The main features of ozone maximum and minimum values are still common to model and observation but the precise positions of the features move apart. Clearly, in the lower stratosphere, the calculated (forecast) dynamical fields drift away from the analyses, leading to a less realistic total-ozone field when compared with observations. Nevertheless, the column-ozone results show that even with a simple chemical initialization realistic composition fields can soon be established in the model, as long as in this case the simple initialization captures the observed zonal mean structure of the atmosphere. For example, in this integration the ozone field agreed with observations by the third day.

Our more recent model developments have included an improved initialization in which the initial 2-D constituent fields are transformed into an 'equivalent potential vorticity latitude–potential temperature' coordinate system (Lary *et al.* 1994, private communication), which should lead to significant improvements. Nevertheless, for the purposes of this paper, the zonally symmetric initialization is perfectly acceptable.

(*c*) O_3 *mixing ratios at* 10 *mb*

Figure 9 shows the development of the ozone field at 10 mb during the integration. Figure 9(b), 12 hours after the start of the run, shows that the strong cross-polar flow has pushed the ozone minimum well off the pole, towards 60°N, 60°W. Thirty-six hours later (Fig. 9(c)) a horseshoe shape has been established, quite unlike the initial conditions.

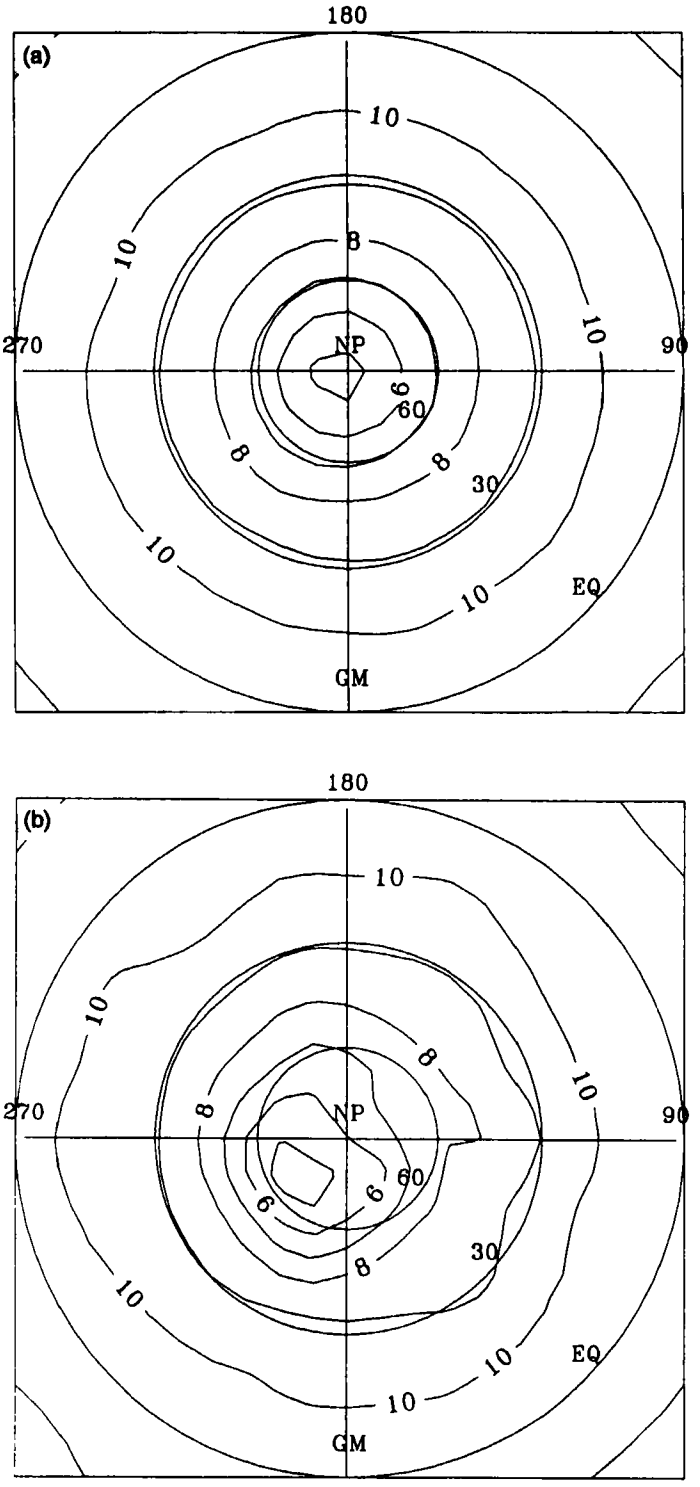

Figure 9. Modelled ozone mixing ratio (p.p.m.v.) at 10 mb in the northern hemisphere for: (a) 1400 GMT 15 January 1987, (b) 0000 GMT 16 January 1987, (c) 1200 GMT 17 January 1987 and (d) 1200 GMT 21 January 1987.

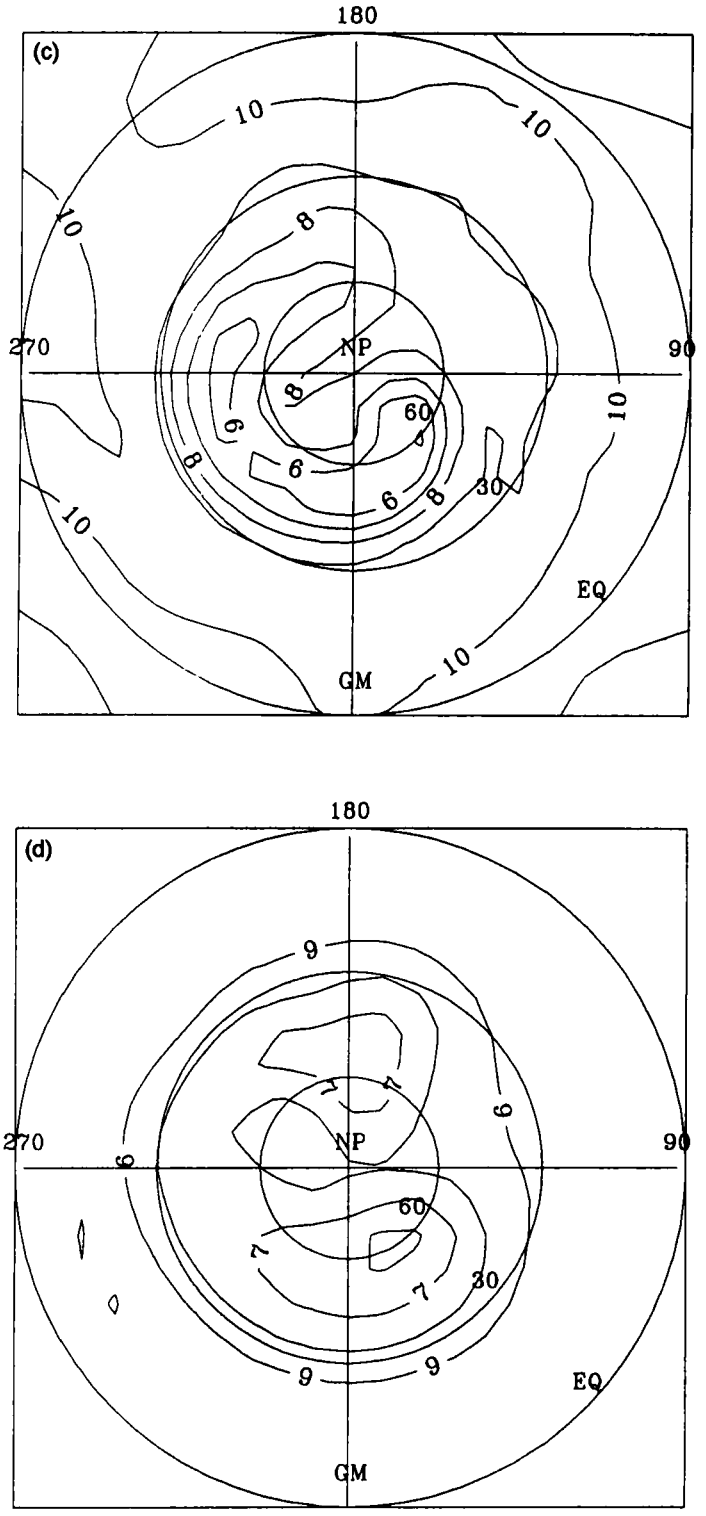

Figure 9. Continued.

By 21 January (Fig. 9(d)) the original minimum has been split into two, with one centred over the vortex at 60°N, 40°E and the secondary minimum being close to the Aleutian anticyclone. (Calculations with the improved chemical initialization do not show this second minimum.) In between the minima lies a region of higher mixing ratios over the pole, air that has been advected from lower latitudes.

Figure 9(c) is reminiscent of the Limb Infra-red Monitor of the Stratosphere (LIMS) ozone fields during January and February 1979 studied by Leovy *et al.* (1985). Figure 10, based on their paper, traces with a dashed line the tongue of low-latitude air, poor in ozone, that has been pulled towards the North Pole at 10 mb. It seems clear that the features shown in Figs. 9 and 10 are similar.

(*d*) *Column NO_2*

The vertical column of NO_2 from 15 January is shown in Fig. 11. Initialization from the 2-D model leads to a zonally symmetric field for the odd-nitrogen family (NO_x in Table 2). Figure 11 shows a highly non-zonal field for NO_2 that arises because the rapid chemical partitioning within the odd nitrogen family varies with zenith angle. Thus a dominant feature is the terminator that crosses the lower (Atlantic) side of the map. In the sunlit portion of the globe, NO_2 levels are generally low while night-time values are high, even over the pole.

Figure 12(a) shows the same field a few days later on 19 January. Again the variation across the terminator stands out strongly. Following, for example, the 45°N latitude circle anticlockwise from dawn to dusk, note the general increase in NO_2 associated with its

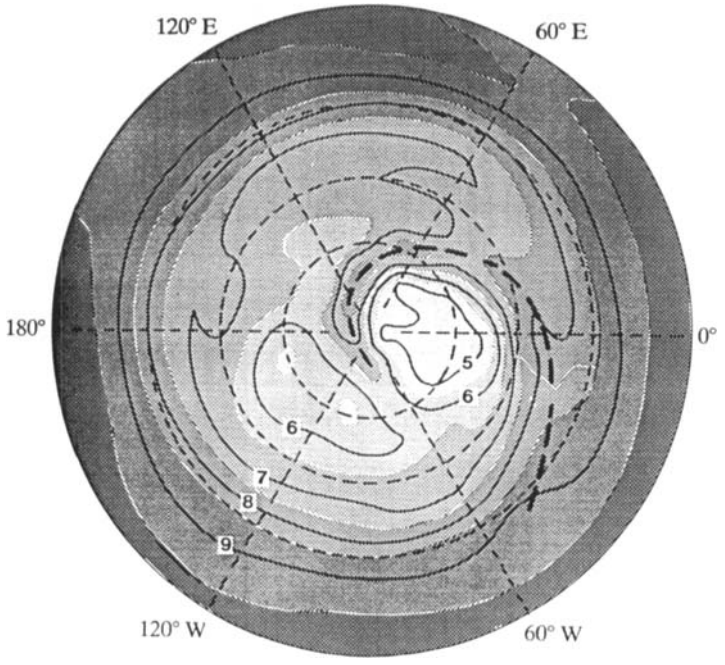

Figure 10. Ozone mixing ratio (p.p.m.v.) on the northern hemisphere 10 mb surface on 6 February 1979 as measured by the Nimbus 7 Limb Infra-red Monitor of the Stratosphere (LIMS) instrument. (Figure produced by J. C. Farman for *Phil. Trans. R., Soc. London A*, 323 after Leovy *et al.* 1985, and reproduced with

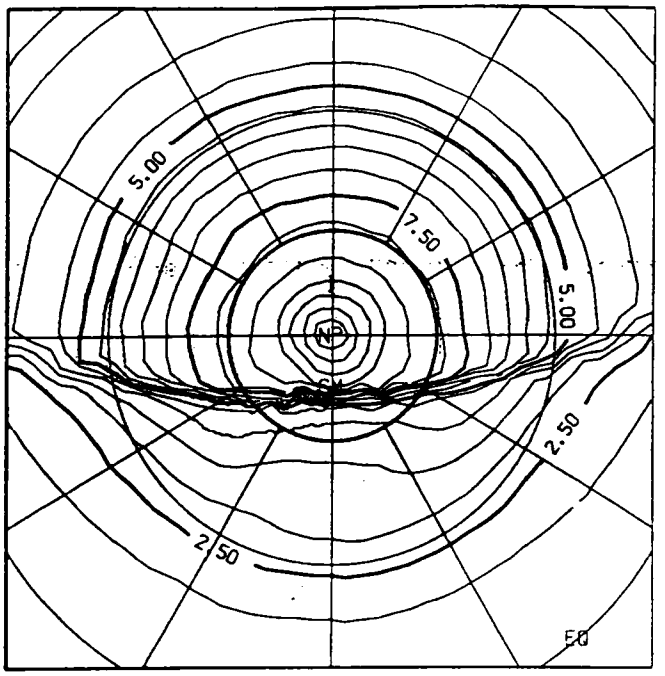

Figure 11. Calculated NO_2 column (10^{15} molecules cm^{-2}) for the northern hemisphere, 1200 GMT 15 January 1987. The figure shows the initial conditions, before integration.

TABLE 2. SPECIES GROUPINGS USED IN THIS STUDY

Families	**Reservoir species**
$O_x = O(^1D) + O(^3P) + O_3$	N_2O_5, HNO_3, HO_2NO_2, $ClONO_2$, HCl, HOCl
$NO_x = N + NO + NO_2 + NO_3$	
$ClO_x = Cl + ClO + Cl_2O_2$	**Source gases**
$HO_x = H + OH + HO_2$	N_2O, H_2O, CH_4
	F11 ($CFCl_3$), F12 (CF_2Cl_2), F22 (CHF_2Cl)
	F113 ($CF_2ClCFCl_2$), CH_3Cl, CH_3CCl_3, CCl_4

release by photolysis of N_2O_5. Similarly, notice the night-time decay of NO_2 at the same latitude: just after sunset, column NO_2 amounts are at their highest and gradually decay during the night as N_2O_5 is produced. The mid-latitude behaviour of the model is thus in excellent agreement with the observed NO_2 diurnal variation (see Webster *et al.* 1990; Lary *et al.* 1991).

Figure 12(a) shows a very interesting feature, not shown in Fig. 11, when the high-latitude column NO_2 amount drops to very low values (e.g. around 60°N, 90°W). This feature is reminiscent of the Noxon cliff, a feature first measured by the late John Noxon (Noxon 1979; Noxon *et al.* 1979, 1983), in which the column NO_2 can drop dramatically with increasing latitude. Figure 12(b) shows the calculated NO_2 column for 27 January. A Noxon cliff-like feature is again evident, although in this case the lowest values are found over the pole and not displaced to the west as found in Fig. 12(a). Later we will return to a detailed discussion of this behaviour of NO_2 in high latitudes, after first presenting results showing the distribution of the two major nitrogen reservoirs, N_2O_5 and HNO_3.

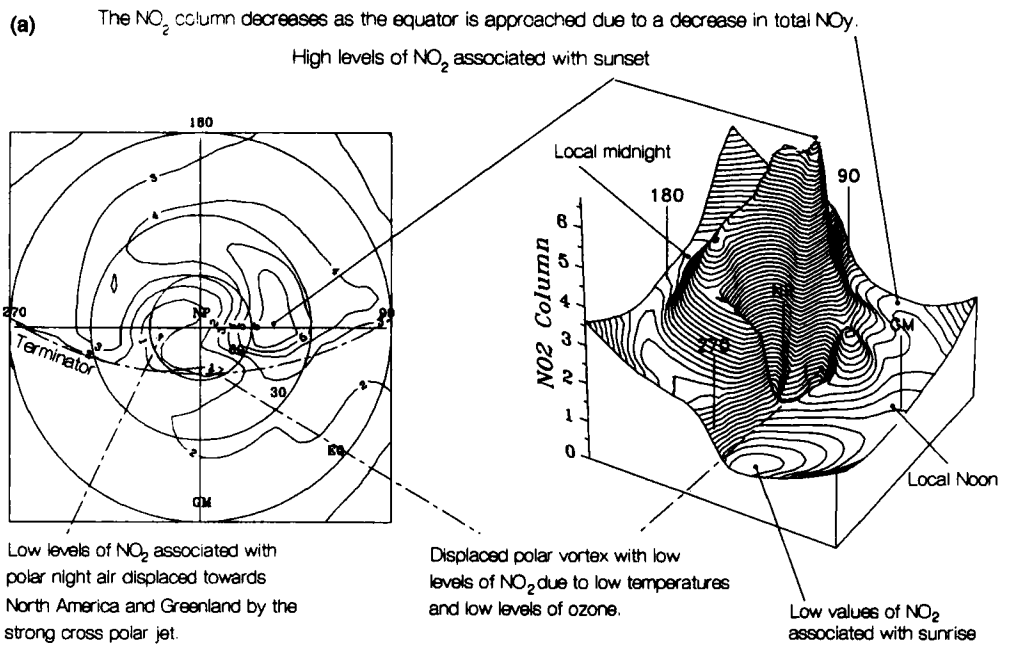

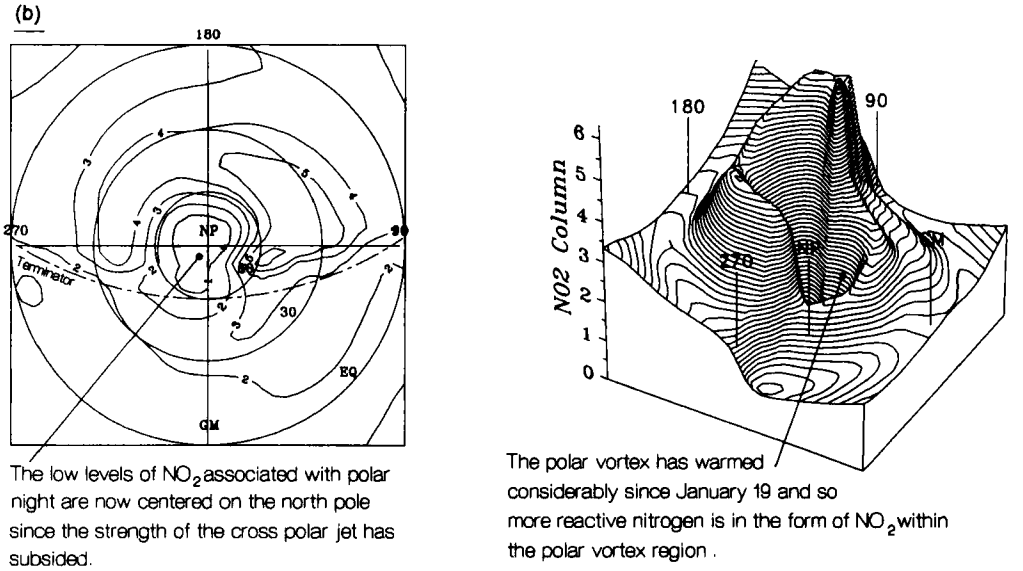

Figure 12. The modelled NO_2 column (10^{15} molecules cm^{-2}) for the northern hemisphere for: (a) 1200 GMT 19 January 1987 and (b) 1200 GMT 27 January 1987. Note: In (a) the sharp gradients in NO_2 are shifted to lower latitudes owing to the presence of a strong cross-polar jet.

(e) N_2O_5

Figure 13 shows the N_2O_5 mixing-ratio fields at 10 mb for 19 and 25 January. The N_2O_5 values are highest in polar regions. When the NO_2 minimum is displaced off the pole on 19 January, so is the N_2O_5 maximum. On 25 January maximum N_2O_5 mixing ratios and minimum NO_2 column (not shown) again coincide, this time over the pole.

Like NO_2, N_2O_5 has a diurnal variation. However, while the NO_2 photochemical time constant is very short, being on the order of minutes, that for N_2O_5 is longer and on the order of hours. Thus, N_2O_5 does not show a strong variation across the terminator. Instead minimum values are found in the late afternoon and into the early part of the night (easily seen following the 30°N latitude circle in Fig. 13(a) when the lowest N_2O_5 is found near 80°E). Minimum values occur following the relatively slow photolysis during the day and before substantial night-time production has taken place. Similarly, large concentrations are found at the end of the night and during the first few hours of sunlight.

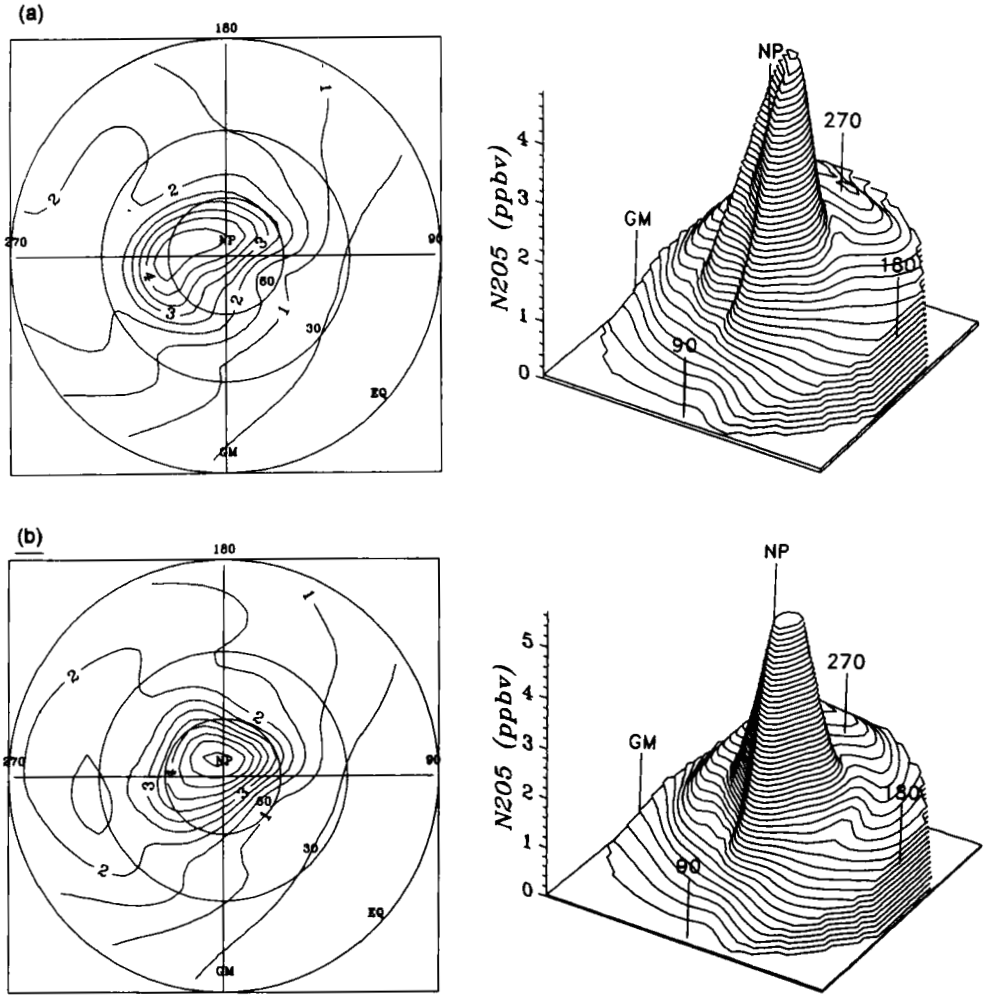

Figure 13. The modelled N_2O_5 mixing ratio (p.p.b.v.) at 10 mb in the northern hemisphere for: (a) 1200 GMT 19 January 1987 and (b) 1200 GMT 25 January 1987.

(f) HNO_3

The ratio of the concentrations of nitric acid to NO_y (defined as the sum of all odd-nitrogen compounds) at 10 mb on 21 January is shown in Fig. 14. There is no strong correlation of HNO_3 with the NO_2 field for the same day. Instead the nitric acid behaviour resembles that of O_3. It is evident that the HNO_3 is influenced after six days of calculation primarily by the initialization and subsequent dynamics, and that chemistry has had only a minor influence on its distribution. However, there is some correspondence between the HNO_3 concentration and the temperature structure. In particular, low HNO_3, relative to NO_y, is found in the warm cross-polar jet.

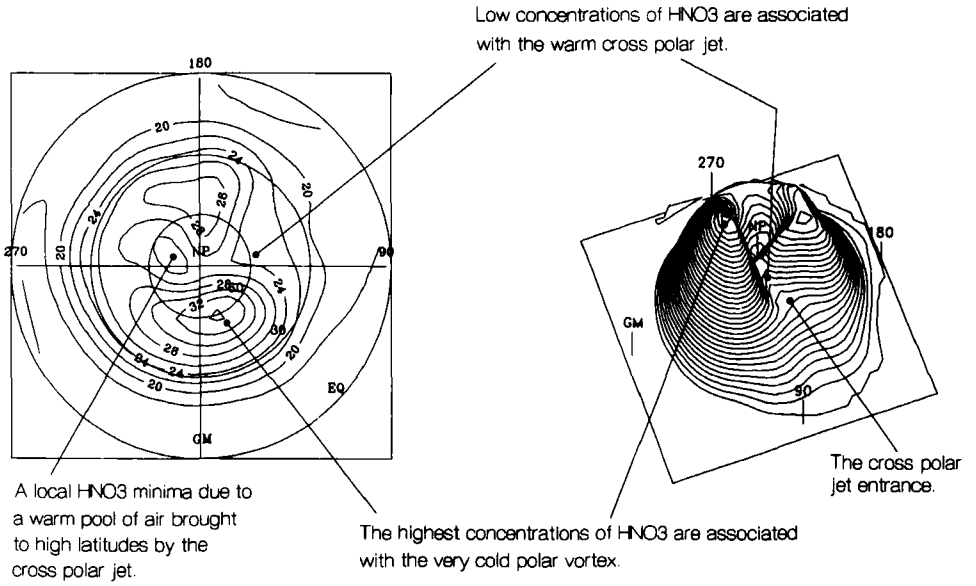

Figure 14. The modelled ratio (%) of HNO_3 to NO_y ($NO_x + HNO_3 + 2N_2O_5$) at 10 mb in the northern hemisphere for 21 January 1987.

5. Discussion

The Noxon cliff was discovered in the late 1970s when a series of measurements of the NO_2 column, made at various times and latitudes, revealed a hitherto unexpected feature (Noxon *et al.* 1979, 1983). Noxon found that in the winter and spring the generally increasing trend of the NO_2 column with latitude could on occasion be dramatically reversed. The NO_2 column could then drop by a large factor from perhaps 7×10^{15} molecules cm^{-2} to less than 10^{15} molecules cm^{-2}, over a few degrees of latitude.

It is clear that the normal partitioning within the nitrogen family is perturbed during these situations. A number of possibilities exist. Firstly, the NO_2 could have been converted to N_2O_5 by the reactions

$$NO_2 + O_3 \rightarrow NO_3 + O_2$$

$$NO_3 + NO_2 + M \rightarrow N_2O_5 + M$$

where production of N_2O_5 is rate limited by the reaction between NO_2 and O_3. This reaction is part of the normal diurnal cycle of NO_2 and would be favoured by long periods of darkness in the polar winter. Slow photolysis of N_2O_5, the main destruction of N_2O_5,

in the cold high-latitude stratosphere could then keep the NO_2 low as the air parcel is advected from high latitudes to the measuring sites. This idea was put forward by, amongst others, Solomon and Garcia (1983a,b) and Callis *et al.* (1983). Solomon and Garcia (1983a) suggested in particular that the details of the cliff might depend strongly on the temperature dependence of N_2O_5 photolysis.

Another possibility suggested by Noxon (1979) is that HNO_3 is the reservoir. HNO_3 is produced by the reaction

$$NO_2 + OH + M \rightarrow HNO_3 + M.$$

This reaction is favoured by low temperatures and requires sunlight to produce the OH radical. HNO_3 could also be the reservoir if heterogeneous reactions are involved. For example,

$$N_2O_5(g) + H_2O(s) \rightarrow 2HNO_3(s)$$

is known to be effective both on nitric acid trihydrate particles (polar stratospheric clouds) and aerosol surfaces (Hanson and Ravishankara 1991). The reaction on polar stratospheric clouds obviously needs the low temperatures required for the formation of these surfaces. The reaction on sulphate aerosol appears to be independent of temperature.

The run considered above includes only gas-phase chemistry so we are unable to say anything about the role of heterogeneous chemistry. However, it is clear that, on the basis of the calculations described in section 4, gas-phase formation of N_2O_5 leads to the modelled Noxon cliff. This is amply demonstrated in Figs. 12 and 13 where there is a very strong anticorrelation in high latitude between NO_2 and N_2O_5. The large area of low NO_2 corresponds exactly to the region of highest N_2O_5 concentration. Furthermore, this is also where the ratio of HNO_3 to NO_y becomes low (Fig. 14). Whether or not HNO_3 would subsequently be formed on sulphate aerosol—temperatures are too high for polar stratospheric clouds to form—it is clear that, under the dynamical conditions of January 1987, formation of N_2O_5 is the precondition for the formation of the Noxon cliff.

To consider the situation in more detail, consider the rate-limiting step for formation of N_2O_5

$$NO_2 + O_3 \rightarrow NO_3 + O_2 \qquad k = 1.2 \times 10^{-15} \exp(-2450/T) \text{cm}^3\text{s}^{-1}$$

where T is temperature, and for its destruction

$$N_2O_5 + h\nu \rightarrow NO_2 + NO_3.$$

It is clear from these two reactions that high concentrations of N_2O_5 are favoured by darkness, when the photolysis of N_2O_5 is zero, and by both high concentrations of ozone and high temperatures, which lead to enhanced rates of production of N_2O_5. All of these conditions are present over the pole in January. One of the major features of the model simulation is a warm cross-polar jet which brings air, rich in ozone, from lower latitudes across the pole and around the edge of the vortex. This is very evident in, for example, Figs. 5(b) and 9(d) which show high temperatures and ozone, respectively, at 10 mb over the pole on 21 January. At the same time, the flow across the pole leads to perhaps 18 hours of darkness for individual air parcels, as revealed by tracer experiments in the model. Under these conditions most of the NO_2 can be removed, as shown schematically in Fig. 15.

The exact position of the cliff can also be explained. On 19 January the cross-polar flow around the vortex was strong, and the low NO_2 was advected away from the pole

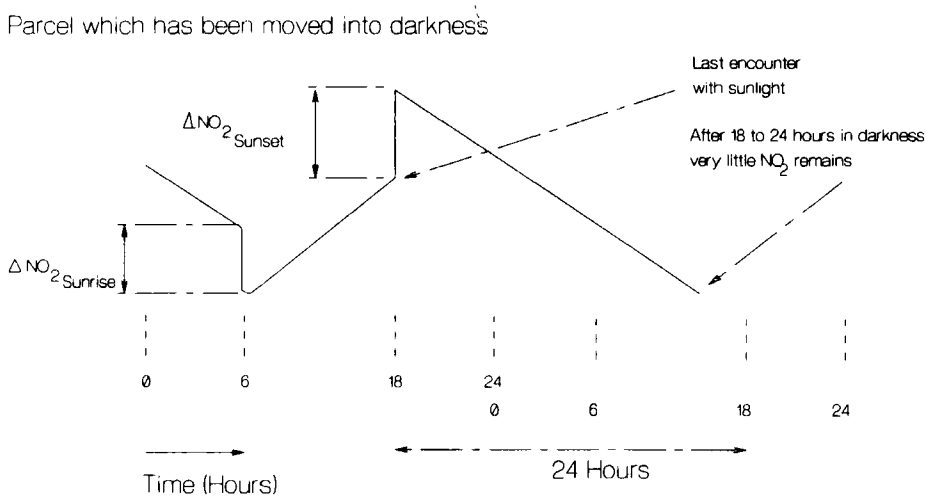

Figure 15. A schematic of the NO_2 diurnal variation. The first 24 hours show the normal mid-latitude variation. The situation when an air parcel crosses into polar night, when much longer periods of darkness may be experienced, is also shown, beginning at 'last encounter with sunlight'.

(see Fig. 12), whereas by 27 January the flow had weakened somewhat and the low NO_2 was most nearly confined to the polar night (Fig. 12(b)).

To test these ideas further, sensitivity calculations were carried out to examine, firstly, the importance of the temperature dependence of the N_2O_5 photolysis in producing the Noxon cliff, as suggested by Solomon and Garcia (1983a), and, secondly, to assess the impact, under the conditions of this calculation, of chemistry on polar stratospheric clouds (PSCs).

A second model run was performed to assess the sensitivity of the NO_2 concentration to the temperature-dependent N_2O_5 absorption cross-section. The basic run, described earlier, included the temperature-dependent N_2O_5 absorption cross-section; the second run kept the cross-section fixed at its 273 K values. When the temperature dependence is included, the N_2O_5 photolysis rate increases with temperature. The model temperature in the region where NO_2 peaks ($\approx$ 10 mb, or 30 km) is around 200 K, and the use of the temperature-dependent cross-section gives a slower photolysis rate than if the 273 K cross-section were used. In consequence, the amplitude of the modelled N_2O_5 diurnal cycle is less when temperature dependence is included and, as a result, equatorward of the polar-night boundary the peak in the NO_2 concentration, which occurs just after sunset, is lower. At 10 mb the largest difference in NO_2 concentration between the two runs was approximately 1.7 parts per billion (10^9) by volume (p.p.b.v.) at close to 70°N, accompanied by a slight decrease in $ClONO_2$ and a corresponding increase in N_2O_5.

Two points are noteworthy. Firstly, it is clear that the use of the temperature-dependent N_2O_5 absorption cross-section did not lead to the Noxon cliff. When the cross-section was kept fixed at its 273 K values the shape and location of the features in the NO_2 column did not change, but the peak NO_2 column just after sunset was simply reduced by approximately 1.5×10^{15} molecules cm^{-2} (comparable with the calculations of Solomon and Garcia (1983a)). Secondly, there was virtually no change in the NO_2 concentrations in the polar-night region, emphasising that the reaction $NO_2 + O_3 \rightarrow NO_3 + O_2$, followed by the formation of N_2O_5, is 'complete' in approximately 18

to 24 hours at 10 mb (Lary 1991). Thus it is the extended period of darkness experienced by air parcels in the polar night that lead to the Noxon cliff.

Model runs were also performed to assess the sensitivity of the NO_2 concentration to heterogeneous reactions on PSCs. For this simulation of January 1987 the inclusion of reactions on PSCs made very little difference to the calculated NO_2 column, simply because the temperatures were not cold enough for their formation where the NO_2 concentration peaks (≈ 10 mb). If the temperatures had been cold enough then sharp spatial gradients in the NO_2 column could easily have been generated by the reactions on PSCs. This will be examined in future calculations for different periods.

Reactions on sulphate aerosols, particularly the reaction $N_2O_5 + H_2O \rightarrow 2HNO_3$, would decrease the NO_2 concentration. However, this would be most important in the lower stratosphere where the aerosol layer peaks, but below where NO_2 peaks. In addition, as the aerosol layer generally covers a wider area than the region of cold temperatures producing PSCs, the modification of the NO_2 column by reactions on sulphate aerosols are themselves more likely to cover a larger area than those caused by PSCs. Thus, on their own, reactions on sulphate aerosol seem unlikely to generate sharp spatial gradients in NO_2.

6. Conclusions

A new 3-D photochemical model of the stratosphere has been described. The model is based on the spectral GCM being developed by the UK UGAMP. To this has been added schemes for tracer advection, gas-phase chemistry, and photochemistry.

The model was integrated for a two-week period in January 1987. The modelled total ozone, despite a very simple chemical initialization, agrees well with the observed TOMS fields, demonstrating the very good dynamical performance of the model.

The model reproduces a feature resembling the Noxon cliff, with very low NO_2 over the pole. A combination of dynamical and chemical processes lead to the formation of the cliff. Gas phase conversion of NO_2 to N_2O_5 occurs in the model, favoured by the high ozone and high temperatures as air moves around the poleward flank of the vortex at 10 mb. These air parcels are subject to long periods of darkness, with no photolysis on N_2O_5, so that the formation of N_2O_5 is essentially complete in approximately 18–24 hours at 10 mb (Lary 1991).

The sensitivity to both heterogeneous chemistry and the temperature dependence of the N_2O_5 photolysis was studied. Under the conditions of the model run, the reactions on polar stratospheric clouds played a negligible role. Inclusion of the N_2O_5 temperature dependence led to a smaller peak in the NO_2 column just after sunset, with the reduced N_2O_5 photolysis rate causing an NO_2 diurnal cycle of reduced amplitude. The temperature-dependent N_2O_5 absorption cross-section did not generate the Noxon cliff in the model, and did not significantly affect the shape or location of spatial gradients in the NO_2 column.

Acknowledgements

This work is part of the UK Universities Global Atmospheric Modelling Programme funded by the Natural Environment Research Council. We acknowledge the support of DGXII of the Commission of the European Communities under STEP 013 and STEP 016. Dr G. Carver is supported by UGAMP. Part of this work was carried out while Dr Lary was supported by a Science and Engineering Research Council studentship. We thank the ECMWF for the original version of the tracer advection code. Special thanks

must be given to the UGAMP core group at the University of Reading. The TOMS data were taken from the CD ROM of gridded data for 1978–88, provided by the Goddard Ozone Processing Team, December 1990 (P. Guimaraes and R. McPeters, Eds).

References

Allen, M. and Frederick, J.E. 1982 Effective photodissociation cross sections for molecular oxygen and nitric oxide in the Schumann to Runge bands. *J. Atmos. Sci.*, **39**, 2066–2075

Anderson, D. E. 1983 The troposphere to stratosphere radiation field at twilight: a spherical model. *Planet. Space Sci.*, **31**, No. 12, 1517–1523

Asselin, R. 1982 Frequency filter for time integrations. *Mon. Weather Rev.*, **100**, 487–490

Austin, J. 1991 On the explicit versus family solution of the fully diurnal photochemical equations of the stratosphere. *J. Geophys. Res.*, **96**, 12941–12974

Austin, J. and Butchart, N. 1992 A three-dimensional modelling study of the influence of planetary wave dynamics of polar ozone photochemistry. *J. Geophys. Res.*, **97**, 10165–10186

Callis, L. B., Russell III, J. M., Haggard, K. V. and Natarajan, M. 1983 Examination of wintertime latitudinal gradients in stratospheric NO_2 using theory and LIMS observations. *Geophys. Res. Lett.*, **10**, 945–948

Cariolle, D. and Deque, M. 1986 Southern Hemisphere medium-scale waves and total ozone disturbances in a spectral general circulation model. *J. Geophys. Res.*, **91**, 10825–10846

Carver, G. C., Norton, W. and Pyle, J. A. 1994 Forecasting the disturbed stratospheric Arctic vortex of January 1992. *Geophys. Res. Lett.*, in Press

Crutzen, P. J. 1971 Ozone production rates in an oxygen, hydrogen, nitrogen-oxide atmosphere. *J. Geophys. Res.*, **76**, 7311–7327

DeMore, W. B., Molina, M. J., Sander, S. P., Golden, D. M., Hampson, R. F., Kurylo, M. J., Howard, C. J. and Ravishankra, A. R. 1987 'Chemical kinetics and photochemical data for use in stratospheric modelling'. Evaluation number 8, NASA JPL Publication 87–41

1990 'Chemical kinetics and photochemical data for use in stratospheric modelling'. Evaluation number 9, NASA JPL Publication 90–1

Dobson, G. M. B., Harrison, D. N. and Lawrence, J. 1927 Measurements of the amount of ozone in the earth's atmosphere and its relation to other geophysical conditions: Part II. *Proc. R. Soc. London*, **A114**, 521–541

Douglass, A. R., Jackman, C. H. and Stolarski, R. S. 1989 Comparison of model results transporting the odd nitrogen family with results transporting separate odd nitrogen species. *J. Geophys. Res.*, **94**, 9862–9872

Geleyn, J. F. and Hollingsworth, A. 1979 An economical analytical method for the computation of the interaction between scattering and line absorption of radiation. *Beitr. Phys. Atmos.*, **52**, 1–16

Geleyn, J. F., Hense, A. and Preuss, H. J. 1982 A comparison of model generated radiation fields with satellite measurements, *Beitr. Phys. Atmos.*, **55**, 253–286

Granier, C. and Brasseur, G. 1991 Ozone and other trace gases in the Arctic and Antarctic regions: three-dimensional model simulations. *J. Geophys. Res.*, **96**, 2995–3011

Grose, W. L., Nealy, J. E., Turner, R. E. and Blackshear, W. T. 1987 Modelling the transport of chemically active constituents in the stratosphere, Pp. 229–250 in *Transport processes in the middle atmosphere*. D. Reidel, Hingham, Mass

Hanson, D. R. and Ravishankara, A. R. 1991 The reaction probabilities of $ClONO_2$ and N_2O_5 on 40% to 75% sulphuric acid solutions. *J. Geophys. Res.*, **96**, 17307–17314

Harwood, R. S. and Pyle, J. A. 1975 A two-dimensional mean circulation model for the atmosphere below 80 km. *Q. J. R. Meteorol. Soc.*, **101**, 723–747

Hoskins, B. J. and Simmons, A. J. 1975 A multi-layer spectral model and the semi-implicit method. *Q. J. R. Meteorol. Soc.*, **101**, 637–655

Johnston, H. S. 1971 Reduction of stratospheric ozone by nitrogen oxide catalysts from supersonic transport exhaust. *Science*, **173**, 517–522

Kaye, J. A. and Rood, R. B. 1989 Chemistry and transport in a three-dimensional stratospheric model: Chlorine species during a simulated stratospheric warming. *J. Geophys. Res.*, **94**, D1, 1057–1083

Kuo, H. L. 1974 Further studies of the parametrization of the influence of cumulus convection on large scale flow. *J. Atmos. Sci.*, **31**, 1232–1240

Lacis, A. A., Wuebbles, D. J. and Logan, J. A. 1990 Radiative forcing of climate by changes in the vertical distribution of ozone. *J. Geophys. Res.*, **95**, 9971–9981

Lary, D. J. 1991 'Photochemical studies with a three-dimensional model of the atmosphere'. PhD thesis, University of Cambridge

Lary, D. J. and Pyle, J. A. 1991a Diffuse radiation, twilight, and photochemistry—I. *J. Atmos. Chem.*, **13**, 373–392

1991b Diffuse radiation, twilight, and photochemistry—II. *J. Atmos. Chem.*, **13**, 393–406

Lary, D. J., Pyle, J. A., Webster, C. R. and May, R. D. 1991 The BLISS measurements of NO_2: Some new insights. *Geophys. Res. Lett.*, **18**, 2261–2263

Leovy, C. P., Sun, C-R, Hitchman, M. H., Remsberg, E. E., Russell III, J. M., Gordley, L. L., Gille, J. C. and Lyjak, L. V. 1985 Transport of ozone in the middle stratosphere: Evidence for planetary wave breaking. *J. Atmos. Sci.*, **42**, 230–244

Mahlman, J. D. and Moxim, W. J. 1978 Tracer simulation using a global general circulation model: Results from mid-latitude instantaneous source experiment. *J. Atmos. Sci.*, **41**, 2029–2051

Meier, R. R., Anderson, D. E. and Nicolet, M. 1982 The radiation field in the troposphere and stratosphere from 240 to 1000 nm: general analysis. *Planet. Space Sci.*, **30**, 923–933

Molina, M. J. and Rowland, F. S. 1974 Stratospheric sink for chlorofluromethanes: chlorine atom catalyzed destruction of ozone. *Nature*, **249**, 810–814

Murgatroyd, R. J. 1982 Recent progress in studies of the stratosphere. *Q. J. R. Meteorol. Soc.*, **108**, 271–312

Naujokat, B., Labitzke, K., Lenschow, R., Petzoldt, K. and Wohlfart, R. C. 1987 The stratospheric winter 1986/87: A major midwinter warming 35 years after they were first detected. Beilage zur Berliner Wetterkarte, 56/87 SO 9/87

Nicolet, M. and Kennes, R. 1986 Aeronomic problems of the molecular oxygen photodissociation. I. The O_2 Herzberg continuum. *Planet. Space. Sci.*, **34**, No. 11, 1043–1059

Noxon, J. F. 1979 Stratospheric NO_2, 2. Global behaviour. *J. Geophys. Res.*, **84**, 5067–5076

Noxon, J. F., Whipple Jr, E. C. and Hyde, R. S. 1979 Stratospheric NO_2, 1. Observational method and behaviour at mid-latitude. *J. Geophys. Res.*, **84**, 5047–5065

Noxon, J. F., Henderson, W. R. and Norton, R. B. 1983 Stratospheric NO_2, 3. The effects of large scale horizontal transport. *J. Geophys. Res.*, **88**, 5240–5248

Pyle, J. A. 1980 A calculation of the possible depletion of ozone by chloroflurocarbons using a two-dimensional model. *Pure Appl. Geophys.*, **118**, 355–377

Rood, R. B. 1987 Numerical advection algorithms and their role in atmospheric transport and chemical models. *Rev. Geophys.*, **25**, 71–100

Rood, R. B., Kaye, J. A., Douglass, A. R., Allen, D. J., Steenrod S. and Larson, E. M. 1990 Wintertime nitric acid chemistry: Implications from three-dimensional model calculations. *J. Atmos. Sci.*, **47**, 2696–2709

Simmons, A. J. and Burridge, D. M. 1981 An energy and angular momentum conserving finite difference scheme and hybrid vertical coordinates. *Mon. Weather Rev.*, **109**, 758–766

Simon, P. C., Gillotay, D., Vanlaethem-Meurre, N. and Wisemberg, J. 1988 Ultraviolet absorption cross-sections of chloro- and chlorofluoro-methanes at stratosphere temperatures. *J. Atmos. Chem.*, **7**, 107–135

Solomon, S. and Garcia, R. R. 1983a On the distribution of nitrogen dioxide in the high latitude stratosphere. *J. Geophys. Res.*, **88**, 5229–5239

1983b Simulation of NO_x partitioning along isobaric parcel trajectories. *J. Geophys. Res.*, **88**, 5497–5501

Thuburn, J. 1993 Use of a flux-limited scheme for vertical advection in a GCM. *Q. J. R. Meteorol. Soc.*, **119**, 469–487

Tiedtke, M. 1983 'The sensitivity of the time-mean large scale flow to cumulus convection in the ECMWF model'. Pp. 297–316 in Proceedings of the ECMWF workshop on convection in large-scale models, Reading

Tibaldi, S., Palmer, T. N., Brankovic, C. and Cubasch, U. 1990 Extended range predictions with ECMWF models. II: Influence of horizontal resolution on systematic errors and forecast skill. *Q. J. R. Meteorol. Soc.*, **116**, 835–866

Vaughan, G. and Price, J. D. 1991 On the relation between total ozone and meteorology. *Q. J. R. Meteorol. Soc.*, **117**, 1281–1298

Webster, C. R., May, R. D., Toumi, R. and Pyle, J. A. 1990 Active nitrogen partitioning and the nighttime formation of N_2O_5 in the stratosphere: Simultaneous in situ measurements of NO, NO_2, HNO_3, O_3 and N_2O using the BLISS diode laser spectrometer. *J. Geophys. Res.*, **95**, 13851–13866

WMO 1986 Atmospheric ozone 1985. Assessment of our understanding of the processes controlling its present distribution and change. World Meteorological Organization Global Ozone Research and Monitoring Project, Report No. 16